2024 IEEE International Conference on Robotics and Automation (ICRA 2024)
May 13-17, 2024. Yokohama, Japan

Analyzing Accessibility in Robot-Assisted Vitreoretinal Surgery: Integrating Eye Posture and Robot Position

Satoshi Inagaki[1*], Alireza Alikhani[2], Nassir Navab[3], Mathias Maier[2] and M. Ali Nasseri[2,3,4]

***Abstract*— Several robotic frameworks have been recently developed to assist ophthalmic surgeons in performing complex vitreoretinal procedures such as subretinal injection. However, in order to intuitively integrate robots into the surgical workflow, it is crucial to emphasize that an accessibility analysis framework for vitreoretinal surgery must be considered as an essential component. Such a framework, ideally, considers the comprehensive factors of the eye anatomy and its positioning, the insertion point, and the initial pose and position of the robot. By combining the mobilization of the eyeball and adjusting the pose and position of the robot, the accessibility of such systems is significantly optimized. At the same time, the accessible-visible area is better and faster matched to the working volume of the robot. This paper presents an analysis of an expansion strategy for the robot's accessibility and visibility area. The outcomes of this method demonstrate the promising potential to enhance the robot's accessibility, as evidenced in our analytical and experimental findings from 22.4% to 99.0% of the required working area on an adjustable phantom model.**

***Index Terms*— Medical Robots and Systems; Surgical Robotics: Planning, Robot-Assisted Microsurgery**

I. Introduction

Retinal surgery is a highly intricate medical procedure that demands extraordinary precision and fine motor skills from ophthalmic surgeons. Subretinal injection, retinal vein cannulation, and retinal peeling are examples. In retinal vein cannulation, the surgeon needs to insert the instrument into the vessel whose diameter is 100 μm to 400 μm and keep the position for several minutes [1]. However, human physiology inherently includes minute physiological tremors, making achieving absolute precision consistently challenging. Therefore, the medical field has embraced the concept of robotic platforms to augment and enhance the capabilities of surgeons during retinal surgery [2]–[7].

In clinical situations, the surgeons often rotate patient's eyeballs to move the visible and accessible areas, as demonstrated in Fig. 1. Therefore, flexibility for eye rotation and accessibility to reach the whole operating area in the visible area are also crucial for vitreoretinal surgical robots. In considering the flexibility and accessibility of the surgical robot, one of the most essential requirements is the remote

This work is partially supported by NSK Ltd. Corresponding author: M. Ali Nasseri (ali.nasseri@mri.tum.de)

[1] Inagaki is with NSK Ltd., Japan.

[2]S.A. Alikhani, M. Maier and M. Ali Nasseri are with Augenklinik und Poliklinik, Klinikum rechts der Isar der Technische Universität München, München 81675 Germany.

[3] N. Navab is with Department of Computer Science in Technische Universität München, München 85748 Germany.

[4] M. Ali Nasseri is with the Department of Biomedical Engineering, University of Alberta, Canada.

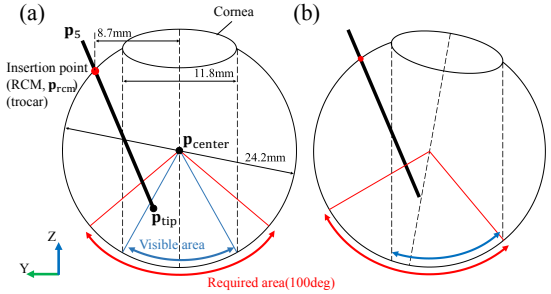

Fig. 1: The effect of rotating eyeball. (a) presents the schematic diagram of the eyeball without tilting. The visible area is moved by rotating the eyeball as shown in (b).

center of motion (RCM) mechanism. The robot has to manipulate the instrument around the insertion point to minimize the damage to the eyeball. When the eyeball rotates, the insertion point will also move; therefore, the robots require the flexibility to follow this shift of the insertion point. There are mainly two types of RCM mechanisms: hardware-RCM (HRCM) and software-RCM (SRCM). In the case of HRCM robots, the mechanical design ensures that the RCM point is consistently located at a specific point, providing a large working volume. Consequently, many research groups have favored this RCM mechanism for conducting vitreoretinal robotic surgery [8]–[10]. However, HRCM robots lack the flexibility to rotate the eyeball due to their fixed mechanical configuration. Conversely, the SRCM mechanism offers to adjust the RCM point with the robot's software, but this adaptability reduces reliability. Among the SRCM robots, the parallel link mechanism is popular because of its compactness, high rigidity, and high accuracy, which are essential for vitreoretinal surgery [11], [12], furthermore, multiple research groups, including ours, have developed this type of robots [13]. Nonetheless, one drawback of this mechanism is its limited working volume compared to the requirements of the HRCM-based robots. The defined required working space of the parallel link SRCM robots are 7 mm in diameter [11] and $\pm$20 deg around the center(8.3 mm in diameter) [14], respectively. On the other hand, regarding the HRCM robots, Gijbel et al. [8] defined the required working volume as 90 deg and Wu et al. [15] defined it 100 deg due to the wide range the various microscope's magnification. It is important to note that the surgical target areas vary depending on the type of operation being performed and the surgical site shift from one surgery to another. As a result, the robot must be adaptable to adjust to these changes [16].

During the operation, the practical operative area is the overlapping region of the visible and the accessible area. The

visible area is influenced by the posture of the eyeball, while the accessible area is affected by the position and pose of the robot and the trocar. It is crucial, especially for robots with limited working volumes, to optimize these factors and adjust the visible-accessible area to cover the target area through preoperative planning. To tackle these challenges, this paper proposes an innovative accessibility analysis framework for vitreoretinal surgical robots. The contribution of this paper is firstly to reveal the effect of eyeball tilt on the insertion angle of the instrument to approach the center of the visible area, and secondly, to analyze the accessibility with different poses of the eye and robot, as well as with different insertion points, leading to an expansion of the accessibility. Thirdly, it experimentally validates the visible-accessible retinal area using a realistic eye phantom.

A. Related Work

Several research papers address the topic of eyeball rotation, as the RCM point experiences a shift during the eyeball's rotation, necessitating the robot to follow and adjust to this motion. Smits et al. developed a fixture mechanism for repositioning RCM points [17] in an HRCM-based surgical robot that controls a large working volume. Thus, the focus of the research was more on RCM repositioning rather than accessibility analysis, which was not required. Orbital manipulation specifically refers to the delicate and precise manipulation or adjustment of instruments or tissues within the eye's orbit, therefore, Koyama et al. [18] and the group of [12], [14], [19] have developed algorithms to perform this procedure within an eyeball by utilizing an SRCM-based dual-arm robot. Their focus is also on rotating eyeballs and developing control algorithms rather than comprehensive accessibility analysis. Our group has also analyzed accessibility and developed the method to relocate the RCM point in [20]. Nevertheless, this accessibility analysis has not discussed the effect of the tilting eyeball. To the best of our knowledge, this paper is the first to comprehensively discuss the accessibility of the eyeball with different eyeball and the robot poses.

II. Method

A. Geometry Of Eyeball

The eyeball is assumed as a sphere, and the diameter is 24.2 mm [21], with the cornea diameter of 11.8 mm, and the trocar is placed in a 17.4 mm diameter ring on the sclera. The visible area is usually set at 60 deg around the center of the eyeball by the microscope, which is almost the same as the size of the cornea. The required working area is defined as 100 deg around the center [15] and the eyeball can rotate $\pm$40 deg around the X and Y axis [22]. However, $\pm$10 deg tilt around the X and Y axis is enough to see the required working area because the visible area rotates in the opposite direction of the eyeball, as shown in Fig. 1. Significant ocular rotation leads to large movements of the trocar, which may interfere with the eyelids around the eye; thus, minor eye rotation is preferred, and the robot should be able to access all required areas with a $\pm$10 deg eye tilt.

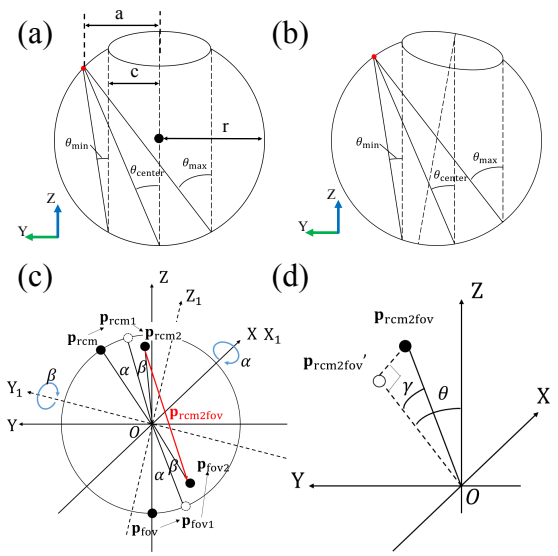

Fig. 2: Insertion angle of the instrument in eye surgery. (a) shows the eyeball without tilt, and (b) shows 10 deg tilt around the X-axis. (c) shows the shift of the insertion point($\mathbf{p}_{\mathrm{rcm}}$) and the center of the visible area($\mathbf{p}_{\mathrm{fov}}$) caused by the rotation around the X and Y axis. (d) represents the insertion angle after rotating the eyeball.

To analyze accessibility, it is required to discuss the effect of eye rotation on the insertion angle to access the visible area. Figure 2(a,b) shows the insertion angle of the instrument with 0 deg and 10 deg tilt around the X-axis respectively. By utilizing the inscribed angle theorem, the insertion angle is calculated. As examples, the calculations of θ_{center} and θ_{min} are shown as follows, where r, a, and c are the eyeball radius (12.1 mm), the insertion ling radius (8.7 mm), and the cornea radius(5.9 mm), respectively.

$$\begin{aligned} \theta_{\mathrm{center}} &= \arcsin(a/r)/2 \\ \theta_{\mathrm{min}} &= (\arcsin(a/r) - \arcsin(c/r))/2 \end{aligned} \tag{1}$$

Through this calculation, the insertion angle is obtained, θ_{center} =23 deg, θ_{min} =8.4 deg, θ_{max} =37.6 deg. These insertion angles do not change by the tilt around the X-axis.

The subsequent phase considers the rotation around the X and Y axis by α and β angle, respectively, as shown in Fig. 2(c). The initial RCM point and the center of the field of view are defined as $\mathbf{p}_{\mathrm{rcm}}$ and $\mathbf{p}_{\mathrm{fov}}$ and these points are shifted to $\mathbf{p}_{\mathrm{rcm1}}$, $\mathbf{p}_{\mathrm{fov1}}$ and then shifted to $\mathbf{p}_{\mathrm{rcm2}}$, $\mathbf{p}_{\mathrm{fov2}}$ by the rotation around the X and Y axis. $\mathbf{p}_{\mathrm{rcm2}}$ and $\mathbf{p}_{\mathrm{fov2}}$ are calculated using the rotation matrix, where $rotx$ and $roty$ are the rotation matrix around the X and Y axis, respectively.

$$\begin{aligned} \mathbf{p}_{\mathrm{rcm2}} &= roty(\beta)rotx(\alpha)\mathbf{p}_{\mathrm{rcm}} \\ \mathbf{p}_{\mathrm{fov2}} &= roty(-\beta)rotx(-\alpha)\mathbf{p}_{\mathrm{fov}} \end{aligned} \tag{2}$$

The insertion vector($\mathbf{p}_{\mathrm{rcm2fov}}$) from $\mathbf{p}_{\mathrm{rcm2}}$ to $\mathbf{p}_{\mathrm{fov2}}$ is driven as follows.

$$\mathbf{p}_{\mathrm{rcm2fov}} = \mathbf{p}_{\mathrm{fov2}} - \mathbf{p}_{\mathrm{rcm2}} \tag{3}$$

Next, the insertion angle θ, γ is defined as illustrated in Fig. 2(d). $\mathbf{p}'_{\mathrm{rcm2fov}}$ is the vector which $\mathbf{p}_{\mathrm{rcm2fov}}$ is projected onto the YZ plane, and θ is calculated from the slope of the $\mathbf{p}'_{\mathrm{rcm2fov}}$ in this plane. Moreover, γ is the angle between

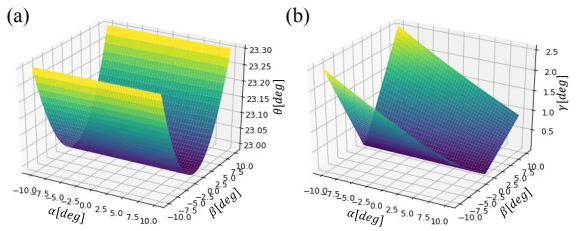

Fig. 3: Insertion angle of the instrument to access the center of the field of view in different postures of the eyeball. (a) and (b) show the change of θ and γ caused by the rotation around the X(α) and Y(β) axis respectively.

$\mathbf{p}'_{\mathrm{rcm2fov}}$ and $\mathbf{p}_{\mathrm{rcm2fov}}$. These two angles can be obtained as follows.

$$\begin{aligned} \theta &= \arctan\left(\frac{\mathbf{p}'_{\mathrm{rcm2fov}}[2]}{\mathbf{p}'_{\mathrm{rcm2fov}}[1]}\right) \\ \gamma &= \arccos\left(\frac{\mathbf{p}_{\mathrm{rcm2fov}} \cdot \mathbf{p}'_{\mathrm{rcm2fov}}}{|\mathbf{p}_{\mathrm{rcm2fov}}||\mathbf{p}'_{\mathrm{rcm2fov}}|}\right) \end{aligned} \tag{4}$$

Consequently, the insertion angle(θ, γ) to access the center of the field of view from the RCM point is derived as shown in Fig. 3 with different tilting angles of the eyeball, α and β from -10 to 10 deg. From this result, θ is almost unchanged from 23 deg, and γ is changed from 0 deg to 2.5 deg. This calculation can be applied to the different insertion and target points.

B. Kinematics And Accessibility Calculation

Firstly, the forward and inverse kinematics are calculated. The forward kinematics [23] of the robot T_j^i is obtained by Denavit–Hartenberg (DH) parameters.

$$\begin{aligned} T_j^i &= A_{i+1}A_{i+2}...A_{j-1}A_j (if\ i < j) \\ A_i &= R_{z,\theta_i} Trans_{z,d_i} Trans_{x,a_i} R_{x,\alpha_i} \end{aligned} \tag{5}$$

where θ_i, a_i, d_i, α_i are parameters associated with $link_i$ and $joint_i$. The inverse kinematics is calculated using the numerical approach (e.g. Jacobian inverse technique) or geometric approach.

The RCM point($\mathbf{p}_{\mathrm{rcm}}$) is along the instrument and can be expressed as follows.

$$\mathbf{p}_{\mathrm{rcm}} = \lambda(\mathbf{p}_{\mathrm{tip}} - \mathbf{p}_5) \tag{6}$$

where $\mathbf{p}_5$ is the endpoint of the last joint of the robot [20] as shown in Fig. 1.

In order to calculate the accessibility, the distance between the tooltip ($\mathbf{p}_{\mathrm{tip}}$) and the center of the eyeball ($\mathbf{p}_{\mathrm{center}}$), which are shown in Fig. 1 should be equal to the radius of the eyeball (r).

$$|\mathbf{p}_{\mathrm{tip}} - \mathbf{p}_{\mathrm{center}}| = r \tag{7}$$

III. Accessibility Analysis

A. Introduction Of The Robot

The whole structure of our surgical robot is shown in Fig. 4(a). Our robot can be divided into two central parts: the 5-DoF robot and the arm robot. The 5-DoF robot is shown in Fig. 4(c). This 5-DoF robot is responsible for the tiny and precise movement of the surgery. The concept design is made by Nasseri et al. [5] and updated by NSK.Ltd. The robot consists of two parallel coupled joint mechanisms (PCJM) for translation and rotation in the X and Y axis and a decoupled prismatic joint for the movement along the Z-axis. This PCJM can be interpreted as a translational and rotational joint serial link. Referring to the kinematic structure in Fig. 4(c), the needle-tip position $\mathbf{p}_{tip}$ is obtained by forward kinematics (Eq. 5) and the inverse kinematics is calculated by a geometric approach [13], [24].

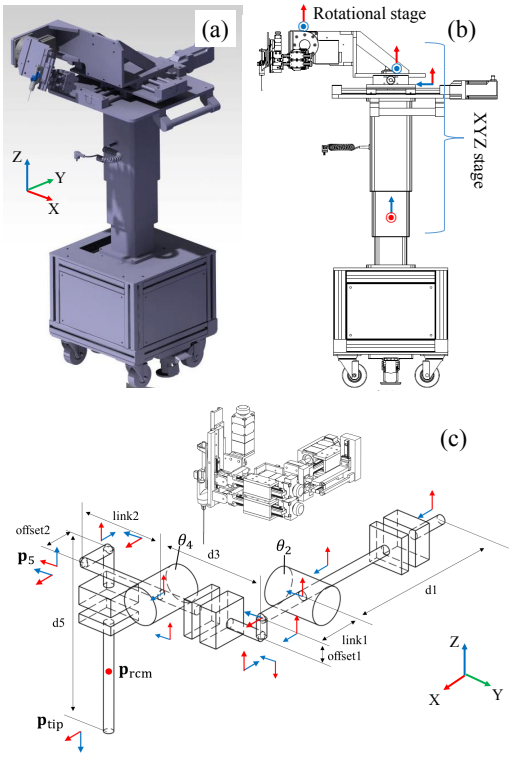

Fig. 4: Kinematic structure of the robot. (a) shows the whole view of the robot. (b) shows the kinematic structure of the arm robot. (c) shows the kinematic structure of the 5-DoF surgical robot.

The arm robot has 4-DoF: X, Y, Z, and θ. This arm robot is responsible for coarse movement. The arm robot brings the 5-DoF robot to the insertion point and tilts the 5-DoF robot to the required angle.

B. Accessibility Analysis

Before starting the accessibility analysis, the default setup should be defined. In the default setup, the eyeball does not rotate($\alpha = \beta = 0$), and the instrument is inserted into the center of the visible area. As explained in Sec. II-A, the insertion angle(θ) to access the center point of the field of view is 23 deg and $\gamma = 0$ deg. The RCM point is set at 20 mm from the tooltip. The arm robot tilts the 5-DoF robot to 23 deg and aligns the RCM point to the insertion point. The insertion point is set at the 3 or 9 o'clock position. Until the arm robot brings the 5-DoF robot to the initial position, the 5-DoF robot does not move, and all the axis is the center of the stroke to maximize the working area. The RCM control and the accessible area can be calculated by Eq. 6 and Eq. 7. As a result, the accessible area in the default setup is obtained,

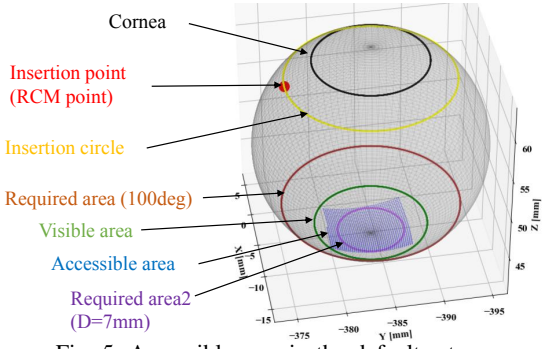

Fig. 5: Accessible area in the default setup.

as shown in Fig. 5. This calculation confirms that our 5-DoF robot meets the Sakai et al. requirement (purple circle, D =7 mm) in the default setup.

Two experimental scenarios are defined to analyze the accessibility. One simulates the case without the compensation of the arm robot. The position of the 5-DoF robot is fixed at the default position. The 5-DoF robot compensates for the movement of the insertion point caused by the eyeball's rotation. The eyeball rotates $\pm$10 deg around the X and Y axis. The second one simulates the case with the compensation of the arm robot. The accessibility is expanded by the combination of rotating the eyeball and adjusting the position of the 5-DoF robot by the arm robot. The arm robot will not only compensate for the movement of the RCM point by the rotation of the eyeball but also change the robot's tilting angle and the insertion point as the following strategy.

As illustrated in Fig. 6, the expanding strategy of the accessibility by adjusting the position of the 5-DoF robot and the accessibility along the X-axis can be expanded by changing the insertion point. As depicted in Fig. 6(a), the arm robot changes the insertion point $\pm$20 deg from the default 9 o'clock position, which leads to about $\pm$3 mm changes along the X-axis. Along the Y-axis, the accessibility can be expanded by tilting the 5-DoF robot 23 $\pm$8 deg as shown in Fig. 6(b).The angle of the robot and the insertion point are defined by considering the geometry of the eyeball explained in Sec. II-A and the accessibility of the default setup. In both cases, it is necessary to calculate the RCM point displacement resulting from the eyeball's rotation, as specified in Eq. 2. The subsequent step is the calculation of the arm robot movement. When the arm changes the tilting angle of the 5-DoF robot, the YZ stage compensates for this tilt. The distance(l) between the center line of the rotational stage($\mathbf{p}_{\text{tilt}}$) and the RCM point($\mathbf{p}_{\text{rcm}}$) is constant because we assumed the 5-DoF robot manipulates the instrument with RCM control and the RCM point is statically fixed. The compensation of the Y and Z stage(y,z) caused by the tilting 5-DoF robot from θ_{before} to θ_{after} can be calculated as follows. θ is the angle between the Z-axis and the line connecting $\mathbf{p}_{\text{rcm}}$ and $\mathbf{p}_{\text{tilt}}$ as demonstrated in Fig. 6(b).

$$
\begin{aligned}
L &= |\mathbf{p}_{\text{rcm}} - \mathbf{p}_{\text{tilt}}| \\
y &= l(\sin(\theta_{\text{after}}) - \sin(\theta_{\text{before}})) \\
z &= l(\cos(\theta_{\text{after}}) - \cos(\theta_{\text{before}}))
\end{aligned} \tag{8}
$$

Thus, the accessible area with the different postures of the eyeball and the position of the insertion point and robot can be calculated. Figure 7 exhibits the changes in the visible area and accessible area when the eyeball is tilted, and the position of the 5-DoF robot is adjusted as explained in Fig. 6. Fig. 7(a) and (c) show the effect of the eyeball rotation around the X and Y axis, respectively. When the eyeball is rotated, the visible area (shown with black and green circles) moves to the edge of the required area (brown) from the center. The accessible area (blue) also moves and stays in the center of the visible area if the insertion point and the tilting angle are not changed. Figure 7(b) and (d) show the effect of changing the insertion point and tilting angle of the 5-DoF robot, respectively. Changing the insertion point (+3 mm along the X-axis) moves the accessible area along the X-axis in the visible area (b). Changing the tilting angle of the 5-DoF robot from 23 deg to 31 deg moves the accessible area along the Y-axis in the visible area (d). It is confirmed by the simulation that the accessible area and visible area are moved by rotating the eyeball and adjusting the position of the 5-DoF robot.

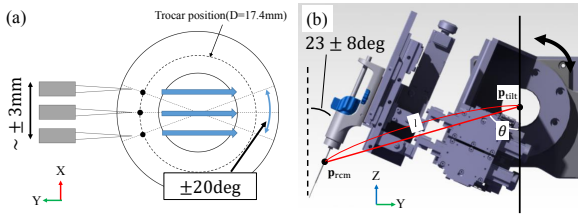

Fig. 6: Strategy to expand the accessible area.

IV. Experimental Evaluation

A. Experimental Method

1) Phantom Eye: In order to evaluate the accessibility of the robot, the phantom eye model is 3D printed as shown in Fig. 8. The bottom part of the eyeball has a grid made of grooves and to visualize the position on the retina. The eye model is capable of rotation by $\pm$10 deg around the X and Y axis, with nine different possible postures. The center of the eye model is designed to keep the position with the different postures. The top part of the eye model contains holes to enable varying insertion points. The 3D-printed jig is also designed to keep the same eye model position for all experiments.

2) Experimental Procedure: First, the eye model and the position of the 5-DoF robot are set to the default setup, while the 5-DoF robot is tilted at 23 deg and the needle is inserted 20 mm from 9 o'clock. The user operated the joystick to the rotational limit of the RCM control or limit of the visible area and then lowered the needle until it stopped in contact with the fundus surface. The eye model is observed by the microscope from the top and taken the photos when the instrument reaches at the fundus. Thus, the measurement of working area of the default setup is completed. Next, the eye model is changed to other different postures and the operator repeats the measurement of the working area. As explained in Sec. III, two scenarios with and without the arm robot are

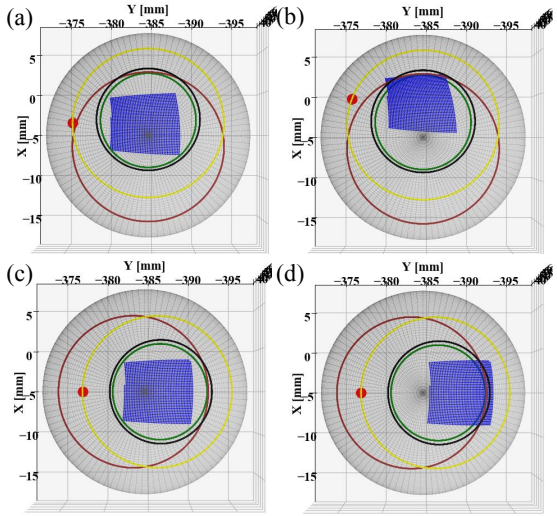

Fig. 7: The effect of tilting eyeball and adjusting the position of 5-DoF robot. (a) shows the accessible area when the eyeball is rotated 10 deg around the Y-axis. (b) The eyeball is rotated, and the insertion point is shifted +3 mm. (c) The eyeball is rotated 10 deg around the X-axis. (d) The eyeball is rotated 10 deg, and the 5-DoF robot is tilted to 31 deg from 23 deg.

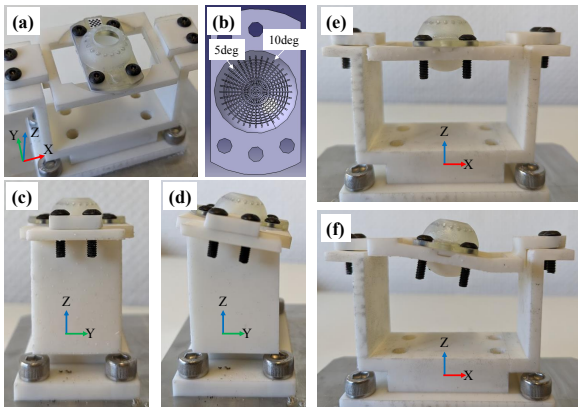

Fig. 8: Eye model to measure the accessibility of the robot. (a) The eye model. (b) The bottom part of the eye model. It has grooves inner side. The radial grooves are every 10 deg. Concentric grooves are every 5 deg. (c)-(f) The two different tilt of the base around the X and Y axis. In each axis, the horizontal and 10 deg tilted base are prepared. The eye model can achieve nine different postures by combining these holders and the eye model is designed so that the center of the eyeball will not change by the postures.

considered. In the case without the arm robot, the arm robot does not move and the 5-DoF robot is fixed at the default position. Therefore, the operator controls the 5-DoF robot to bring the instrument to the insertion point which is shifted by the eyeball rotation. The insertion point is not changed in all postures of the eyeball. In the case of the arm robot, the arm robot compensates for the shift of the eyeball and changes the insertion point and tilting angle of the 5-DoF robot. In order to maximize the total accessibility, when the eyeball rotates ± 10 deg around the Y-axis, the insertion point is also changed ± 3 mm. When the eyeball rotates ± 10 deg around the X-axis, the tilting angle of the 5-DoF robot is changed to 31 deg and 15 deg as shown in Fig. 11(a).

3) Measurement: In the next step, all pixel coordinates (IV-A.2) of the needle tip and all corners of the grid closest

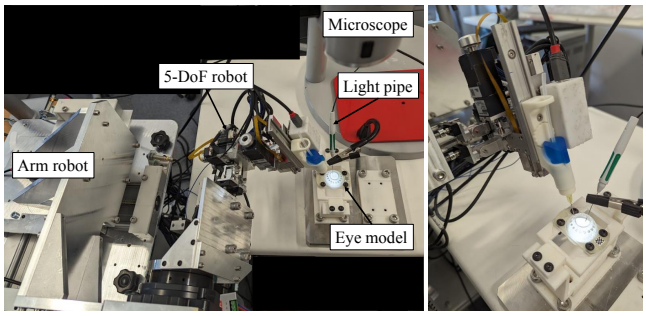

Fig. 9: Experimental setup.

to it were manually collected from all captured images in different orientations of the eye model, as shown in Fig. 10. The polar coordinates of the grid intersections are known and that of the needle tip position(α, β) need to be determined from this information. For simplicity, we assume the radial lines as straight lines and concentric curves as arcs. First, α is calculated as follows. The radius(d_1, d_2) of the arc α_i and α_{i+1} in pixel coordinates are obtained by Eq. 9.

$$\begin{aligned} d_1 &= (|\mathbf{p}_2| + |\mathbf{p}_3|)/2 \\ d_2 &= (|\mathbf{p}_1| + |\mathbf{p}_4|)/2 \end{aligned} \tag{9}$$

The coefficient ϵ to get d_k from d_1, d_2 is derived as follows.

$$\begin{aligned} d_1\epsilon + d_2(1-\epsilon) &= d_k \\ \epsilon &= \frac{d_2 - d_k}{d_2 - d_1} \end{aligned} \tag{10}$$

The difference between α_i and α_{i+1} is 5 deg. Therefore the difference is small enough that the angles are assumed to vary linearly. As a result, α_k is derived as follows.

$$\alpha_k = \alpha_i\epsilon + \alpha_{i+1}(1-\epsilon) \tag{11}$$

In the same way, β_k can be obtained by Eq. 12-14. The slope of the line is the main index for this calculation.

$$\begin{aligned} slope &= \arctan(y/x) \\ \theta_1 &= (slope_1 + slope_2)/2 \\ \theta_2 &= (slope_3 + slope_4)/2 \end{aligned} \tag{12}$$

$$\epsilon = \frac{\theta_2 - \theta_k}{\theta_2 - \theta_1} \tag{13}$$

$$\beta_k = \beta_j\epsilon + \beta_{j+1}(1-\epsilon) \tag{14}$$

The polar coordinates(α_k,β_k) are converted to the cartesian coordinates(x_k,y_k,z_k) as follows.

$$\begin{aligned} x_k &= r\sin(\alpha_k)\cos(\beta_k) \\ y_k &= r\sin(\alpha_k)\sin(\beta_k) \\ z_k &= r\cos(\alpha_k) \end{aligned} \tag{15}$$

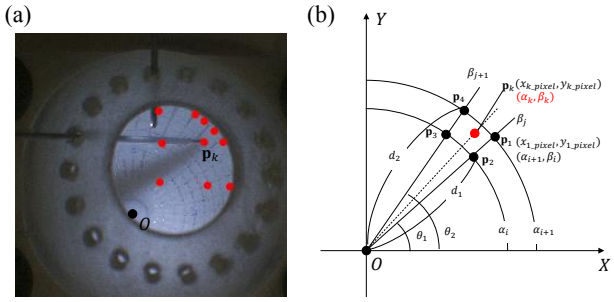

Fig. 10: Accessibility evaluation.(a) shows accessibility of the robot. Red dots shows the edge of the accessible area or the edge of the visible area. (b) shows schematic diagram to calculate the position of the needle tip.

B. Result

Figure. 11(a) shows the experimental result of the case with the arm robot. The red dots represents the edge of the accessible area or the visible area. The field of view is changed as the eye model is rotated and the accessible area is also changed by tilting the 5-DoF robot and inserting position as simulated in Sec. III. From these plots and calculation explained in Sec. IV-A.3, the pixel coordinate of the plots are converted to the real coordinates. Fig. 11(b) and (c) show the simulation and experimental results of the case without and with the arm robot respectively. These plots are combined plots at nine different eye postures and projected to the Z plane for simplicity. The brown circle is the required area and the blue plots are the simulation result and the red dots are derived from the experiment. The experimental results are similar to the analytical results. The simulation results show the coverage rates of the required working area without and with arm robots are 81.6% and 99.0%, respectively. The case without the arm robot shows the expansion of the accessibility caused by the tilting eyeball compared to the cover rate of the default setup, which is 22.4%. The case with the arm robot represents the effect of adjusting the position of the 5-DoF robot and the cover rate improved significantly.

V. Discussion

Through overall accessibility study, we proved that the accessible area can be expanded by rotating the eyeball and adjusting the position of the 5-DoF robot. Furthermore, the tilting angle of the eyeball and the position of the robot can be defined from the target area by this analysis. In this paper, we defined the rotating angle of the eyeball as ± 10 deg, however, increasing the angle of rotation is expected to further increase the accessible area if it is acceptable in clinical situation. From the simulation, the cover rate without the arm robot and ± 15 deg tilting eyeball is 97.8%. In terms of the evaluation method, it's crucial to consider potential sources of error. Firstly, errors may arise from the calculation method, as described in Sec. IV-A.3, where we simplified the radial lines as straight lines and the concentric curves as arcs for the sake of simplicity. Additionally, we assumed that the angle varies linearly within the grid, which is not entirely accurate and introduces some errors. Secondly, manual corrections made to the plots can introduce errors.

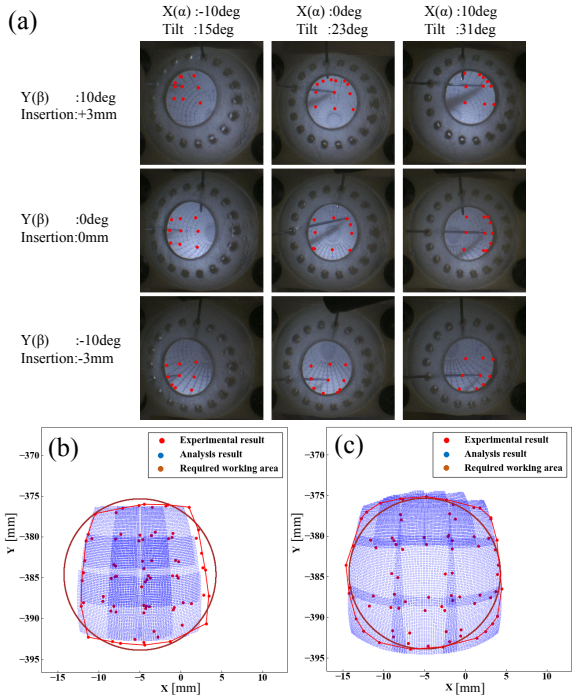

Fig. 11: Accessibility in different eyeball posture. (a) shows the accessibility of the case with arm robot with nine different posture. Red dots represent the the edge of the working area. (b) and (c) show the simulation(blue) and experimental(red) result of the accessible area.(b) shows the case without the arm robot and (c) shows the case with the arm robot.

Thirdly, despite using a jig to align the eye model, there may still be some differences between the eye model, the robot, and the microscope. This misalignment can lead to differences in the visible area compared to the simulation. Lastly, errors stemming from the 3D printer and the straightness of the needle can contribute to inaccuracies. However, for our specific application, these sources of error can be considered negligible, as evidenced by the experimental results.

VI. Conclusion

This paper introduces a comprehensive accessibility study considering various factors, including eye rotation, robot tilt, robot positions, and insertion points. We explain and validate the calculation framework through experiments involving an eye model and robot. By rotating the eyeball within a ± 10 degrees range, the simulation results demonstrate a remarkable expansion of the accessible area, increasing from 22.4% to 81.6%. Furthermore, when combining eyeball rotation with robot position adjustments, the accessible area is significantly enhanced, reaching 99.0%. Future work should address the development of a method to convert fundus image coordinates into real-world coordinates. Additionally, posture detection of the eyeball and control methods for rotating the eyeball are essential for practical applications. Moreover, while our study primarily focuses on accessibility, controlling the injection angle for precise targeting becomes crucial for applications such as injections. In such cases, manipulation of the injection angle through eyeball rotation and insertion point adjustments will also be necessary.

REFERENCES

[1] A. Gijbels, K. Willekens, L. Esteveny, P. Stalmans, D. Reynaerts, and E. Vander Poorten, "Towards a clinically applicable robotic assistance system for retinal vein cannulation," in *2016 6th IEEE International Conference on Biomedical Robotics and Biomechatronics (BioRob)*, pp. 284–291, 2016.

[2] K. Grace, J. Colgate, M. Glucksberg, and J. Chun, "A six degree of freedom micromanipulator for ophthalmic surgery," in *[1993] Proceedings IEEE International Conference on Robotics and Automation*, pp. 630–635 vol.1, 1993.

[3] M. J. Gerber, M. Pettenkofer, and J.-P. Hubschman, "Advanced robotic surgical systems in ophthalmology," *Eye*, vol. 34, no. 9, pp. 1554–1562, 2020.

[4] E. Rahimy, J. Wilson, T. C. Tsao, S. Schwartz, and J. P. Hubschman, "Robot-assisted intraocular surgery: development of the IRISS and feasibility studies in an animal model," *Eye*, vol. 27, no. 8, pp. 972–978, 2013.

[5] M. A. Nasseri, M. Eder, S. Nair, E. C. Dean, M. Maier, D. Zapp, C. P. Lohmann, and A. Knoll, "The introduction of a new robot for assistance in ophthalmic surgery," in *Eng. Med. Biol. Soc. (EMBC), 2013 35th Annu. Int. Conf. IEEE*, pp. 5682–5685, IEEE, 2013.

[6] A. Molaei, E. Abedloo, M. D. de Smet, S. Safi, M. Khorshidifar, H. Ahmadieh, M. A. Khosravi, and N. Daftarian, "Toward the art of robotic-assisted vitreoretinal surgery," *Journal of ophthalmic & vision research*, vol. 12, no. 2, p. 212, 2017.

[7] X. He, D. Roppenecker, D. Gierlach, M. Balicki, K. Olds, P. Gehlbach, J. Handa, R. Taylor, and I. Iordachita, "Toward clinically applicable steady-hand eye robot for vitreoretinal surgery," in *ASME International Mechanical Engineering Congress and Exposition*, vol. 45189, pp. 145–153, American Society of Mechanical Engineers, 2012.

[8] A. Gijbels, N. Wouters, P. Stalmans, H. Van Brussel, D. Reynaerts, and E. V. Poorten, "Design and realisation of a novel robotic manipulator for retinal surgery," in *2013 IEEE/RSJ International Conference on Intelligent Robots and Systems*, pp. 3598–3603, 2013.

[9] J. T. Wilson, M. J. Gerber, S. W. Prince, C.-W. Chen, S. D. Schwartz, J.-P. Hubschman, and T.-C. Tsao, "Intraocular robotic interventional surgical system (iriss): Mechanical design, evaluation, and master–slave manipulation," *The International Journal of Medical Robotics and Computer Assisted Surgery*, vol. 14, no. 1, p. e1842, 2018.

[10] H. Suzuki and R. J. Wood, "Origami-inspired miniature manipulator for teleoperated microsurgery," *Nature Machine Intelligence*, vol. 2, no. 8, pp. 437–446, 2020.

[11] T. Sakai, K. Harada, S. Tanaka, T. Ueta, Y. Noda, N. Sugita, and M. Mitsuishi, "Design and development of miniature parallel robot for eye surgery," in *2014 36th Annual International Conference of the IEEE Engineering in Medicine and Biology Society*, pp. 371–374, IEEE, 2014.

[12] W. Wei, R. E. Goldman, H. F. Fine, S. Chang, and N. Simaan, "Performance evaluation for multi-arm manipulation of hollow suspended organs," *IEEE Transactions on Robotics*, vol. 25, no. 1, pp. 147–157, 2009.

[13] M. A. Nasseri, M. Eder, D. Eberts, S. Nair, M. Maier, D. Zapp, C. P. Lohmann, and A. Knoll, "Kinematics and dynamics analysis of a hybrid parallel-serial micromanipulator designed for biomedical applications," in *2013 IEEE/ASME International Conference on Advanced Intelligent Mechatronics*, pp. 293–299, IEEE, 2013.

[14] W. Wei, R. Goldman, N. Simaan, H. Fine, and S. Chang, "Design and theoretical evaluation of micro-surgical manipulators for orbital manipulation and intraocular dexterity," in *Proceedings 2007 IEEE International Conference on Robotics and Automation*, pp. 3389–3395, 2007.

[15] J. Wu, G. Li, M. Urias, N. A. Patel, Y.-h. Liu, P. Gehlbach, R. H. Taylor, and I. Iordachita, "An optimized tilt mechanism for a new steady-hand eye robot," in *2020 IEEE/RSJ International Conference on Intelligent Robots and Systems (IROS)*, pp. 3105–3111, IEEE, 2020.

[16] K. Faridpooya, S. H. van Romunde, S. S. Manning, J. C. van Meurs, G. J. Naus, M. J. Beelen, T. C. Meenink, J. Smit, and M. D. de Smet, "Randomised controlled trial on robot-assisted versus manual surgery for pucker peeling," *Clinical & experimental ophthalmology*, vol. 50, no. 9, pp. 1057–1064, 2022.

[17] J. Smits, D. Reynaerts, and E. V. Poorten, "Setup and method for remote center of motion positioning guidance during robot-assisted surgery," in *2019 IEEE/RSJ International Conference on Intelligent Robots and Systems (IROS)*, pp. 1315–1322, 2019.

[18] Y. Koyama, M. M. Marinho, and K. Harada, "Vitreoretinal surgical robotic system with autonomous orbital manipulation using vector-field inequalities," in *2023 IEEE International Conference on Robotics and Automation (ICRA)*, pp. 4654–4660, 2023.

[19] H. Yu, J.-H. Shen, K. M. Joos, and N. Simaan, "Design, calibration and preliminary testing of a robotic telemanipulator for oct guided retinal surgery," in *2013 IEEE International Conference on Robotics and Automation*, pp. 225–231, 2013.

[20] M. A. Nasseri, P. Gschirr, M. Eder, S. Nair, K. Kobuch, M. Maier, D. Zapp, C. Lohmann, and A. Knoll, "Virtual fixture control of a hybrid parallel-serial robot for assisting ophthalmic surgery: An experimental study," in *5th IEEE RAS/EMBS International Conference on Biomedical Robotics and Biomechatronics*, pp. 732–738, 2014.

[21] M. Charles and N. Brown, "Dimensions of the human eye relevant to radiation protection (dosimetry)," *Physics in Medicine & Biology*, vol. 20, no. 2, p. 202, 1975.

[22] K. Hoxha, A. Alikhani, S. Inagaki, M. Ferle, M. Maier, and M. A. Nasseri, "Modelling and development of a mechanical eye for the evaluation of robotic systems for surgery,"

[23] M. W. Spong, S. Hutchinson, M. Vidyasagar, *et al.*, *Robot modeling and control*, vol. 3. Wiley New York, 2006.

[24] A. Alikhani, S. Inagaki, J. Yang, S. Dehghani, M. Sommersperger, K. Huang, M. Maier, N. Navab, and M. A. Nasseri, "Pkc-rcm: Preoperative kinematic calibration for enhancing rcm accuracy in automatic vitreoretinal robotic surgery," *IEEE Access*, vol. 11, pp. 103616–103627, 2023.